International Journal of Control, Automation and Systems 15(1) (2017) 362-374
http://dx.doi.org/10.1007/s12555-015-0311-9
ISSN:1598-6446 eISSN:2005-4092
http://www.springer.com/12555

Finite-time H_∞ Adaptive Fault-Tolerant Control for Wing Flutter of Reentry Vehicle Subject to Input Saturation

Ming-Zhou Gao and Guo-Ping Cai*

Abstract: In current study for wing flutter of reentry vehicle, the effect of input saturation to wing flutter is rarely considered and few of the fault-tolerant control problem is taken into account. In this paper, we use the radial basis function neural network and the finite-time adaptive fault-tolerant control technique to deal with the wing flutter problem, which is subject to input saturation, parameter uncertainties and external disturbances. Sensor and actuator faults are both considered in the control design. Firstly, an optimal flight trajectory of reentry vehicle is designed using the conjugate gradient method, so as to decrease the aerodynamic heating rate and temperature on the surface of the reentry vehicle. Then based on the trajectory optimization, we ignore the effect of temperature, and build up the motion equation of wing flutter. Finally, a finite-time H_∞ adaptive fault-tolerant controller is introduced. Simulation results indicate that, the optimized trajectory designed may decrease the aerodynamic heating rate of the reentry vehicle; the designed fault-tolerant controller can effectively deal with the faults in the system and can promptly suppress the wing flutter as well.

Keywords: Fault-tolerant control, finite-time, input saturation, reentry vehicle, wing flutter.

1. INTRODUCTION

During the reentry process of the reentry vehicle, extremely high flight speed leads to serious aerodynamic heating on the surface of the vehicle [1]. To avoid serious surface ablation during the reentry process, temperature protection is a must. One of the possible solutions of reducing the heating rate on the body surface is to use ablative materials [2]. However, due to the complicated behavior of ablative materials and the coupling to the fluid dynamic environment, the study on ablative materials today remains at the level of empirical and the theoretical system for this material is not perfect. Therefore, optimizing the reentry trajectory of reentry vehicle to reduce the heating rate is of greater importance.

Although the optimized reentry trajectory can decrease the heating rate and temperature on the surface of reentry vehicle, aerodynamic load on the surface of reentry vehicle is still very high. It will give rise to more serious wing flutter. Flutter instability may decrease aircraft performance or even lead to the catastrophic failure of the structure [3]. The technique of active flutter suppression has drawn much attention over the past decade [4–7]. For example, Wang *et al*. [4, 5] considered a class of aeroelastic systems with an unmodeled nonlinearity and external disturbance and proposed a full-state feedforward/feedback controller with a high-gain observer; they also designed a continuous robust controller to suppress the aeroelastic vibrations of a nonlinear wing-section model. Zhang *et al*. [6] designed a partial state feedback continuous adaptive controller in order to suppress the aeroelastic vibrations of the wing section model. Cassaro and Battipede [7] considered a class of aeroelastic systems with parameter uncertainties and designed an adaptive control architectures for flutter suppression; they also designed an adaptive controller involves signal filtering in order to improve system performance. Although a number of flutter controller design approaches [3–7], most of the research assume that there exists no actuator fault or failure during the entire flutter suppression. However, the reentry vehicle will face the serious aerodynamic environment in the reentry, the reentry vehicle control systems will inevitably be subjected to the system faults, which are caused by all kinds of actuators, sensors or system components [8]. Thus, the fault tolerant control [9–11] should be token into consideration for the wing flutter.

Fault-tolerant control (FTC) is a control design strategy that guarantees system stability and acceptable per-

Manuscript received August 12, 2015; revised January 6, 2016 and February 19, 2016; accepted March 9, 2016. Recommended by Associate Editor Sing Kiong Nguang under the direction of Editor Fuchun Sun. This work is supported by the Natural Science Foundation of China (11272202, 11132001 and 11472171), the Key Scientific Project of Shanghai Municipal Education Commission (14ZZ021), the Natural Science Foundation of Shanghai (14ZR1421000) and the Special Fund for Talent Development of Minhang District of Shanghai.

Ming-Zhou Gao and Guo-Ping Cai are with the Department of Engineering Mechanics, State Key Laboratory of Ocean Engineering, Shanghai Jiaotong University, 800 Dongchuan Road, Minhang District, Shanghai 200240, China (e-maila: jsycgaomingzhou@163.com, caigp@sjtu.edu.cn).
* Corresponding author.

formance [12]. In general, FTC methods are classified into two types: passive fault tolerant control (PFTC) and active fault tolerant control (AFTC) schemes [12–16]. Xu *et al.* [13] designed an adaptive laws for updating the controller parameters when both the plant parameters and actuator-failure parameters are unknown. Liu *et al.* [14] proposed a novel fault diagnosis architecture for a class of unknown nonlinear systems with unmeasured states; a general radial basis function neural network is used to approximate the unknown system model. Allerhand and Shaked [15] considered as switching in the system dynamics and proposed a fault tolerant control approach to model multiplicative faults. Jia *et al.* [16] constructed a novel fuzzy descriptor learning observer to achieve simultaneous reconstruction of system states and actuator faults; Utilizing the reconstructed fault information, a reconfigurable fuzzy fault-tolerant controller is designed to compensate for the impact of actuator faults. It is worth mentioning that the above researches [12–16] are derived from the assumption that the controllers are able to provide any requested outputs. However, in the reentry process, hypersonic vehicles demand large control forces and signal magnitude, the control actions are usually limited, which means the controller is under actuator saturation. Note that, when physical constraints are in effect, the flutter controller performance will decline because the necessary control signal to achieve the suppression cannot be implemented within the physical constraints imposed on the system [17]. There are several interesting works attempting different adaptive control methods for systems in the presence of actuator saturation [17–19]. Xu *et al.* [18] used fuzzy logic and the disturbance observer to deal with the uncertain nonlinear systems with actuator saturation and external disturbances. Zhong [19] presented a novel method of designing model reference adaptive control for a class of SISO plants which is assumed to be stable and minimum phase with input saturation. However, these references [3–19] are mainly focusing on the problems of linear and nonlinear systems over an infinite-time interval. In the actual reentry process of vehicle, the speed is so large that a small external perturbation can cause sharp increase of flutter amplitude, resulting in catastrophic damage of the vehicle in a very short time. Therefore, it is required that the flutter amplitude do not exceed a certain bound during a fixed finite-time interval. To the best of our knowledge, the studies on finite-time adaptive fault-tolerant control of wing flutter are very limited in the published literature.

In order to reveal the negative effect of the conventional control on the stability of aeroelastic system and considering the influence of faults, actuator saturation, parameter uncertainties and external disturbances, this paper focuses on the design of adaptive fault-tolerant controller for flutter of wing. A two-dimensional cubic structure nonlinearity wing is adopted as structure model in the flutter analysis. This paper is organized as follows. Section 2 presents the flight trajectory optimization of reentry vehicle. Flutter of wing model is given in Section 3. Section 4 presents a finite-time H_∞ adaptive failure compensation controller. Numerical simulations are given in Section 5. Section 6 briefs the conclusions of the research.

2. REENTRY MODEL AND TRAJECTORY OPTIMIZATION OF SPACE VEHICLE

2.1. Reentry trajectory optimization

The dynamic equation of reentry vehicle can be expressed as [20–22]. The space vehicle would experience severe aerodynamic heat and large overload during the reentry flight. So reentry trajectory optimization should be studied so as to improve thermodynamic environment of the reentry vehicle.

2.1.1 Multiple constraints

Equation (1) can be described as

$$\dot{\mathbf{X}} = \mathbf{f}(\mathbf{X}, \bar{\mathbf{u}}, t), \tag{1}$$

where $\mathbf{X}(t) = [V(t),\ \gamma_f(t),\ \psi(t),\ x(t),\ h(t),\ z(t)]^{\mathrm{T}}$ and $\bar{\mathbf{U}}(t) = [\alpha(t),\ \varepsilon(t)]^{\mathrm{T}}$, the subscript T represents the transpose of matrix or vector in this paper.

The multiple constraints for reentry vehicle can be describe as

1) The flying distances x and z should satisfy the following constraints [23]

$$x \le 3500 \text{ km and } z \le -25 \text{ km}. \tag{2}$$

2) The heating rate, dynamic pressure and aerodynamic load must be in the limit as

$$\dot{Q}_n \le \dot{Q}_{n\max} = 420 \text{ kW/m}^2,\ \ q \le 50 \text{ kPa}$$

and

$$n \le n_{\max} = 2.5 \text{ g}. \tag{3}$$

3) The control of reentry vehicle should satisfy the following constraints

$$\begin{cases} \alpha_{\min} = 0^\circ \le \alpha \le \alpha_{\max} = 60^\circ, \\ \varepsilon_{\min} = -60^\circ \le \varepsilon \le \varepsilon_{\max} = 60^\circ. \end{cases} \tag{4}$$

4) The initial and terminal conditions are given as

$$\begin{aligned} &V(t_0) = V_0, \quad \psi(t_0) = \psi_0, \quad x(t_0) = x_0, \\ &h(t_0) = h_0, \quad z(t_0) = z_0, \quad V(t_f) = V_f, \\ &\psi(t_f) = \psi_f, \quad x(t_f) = x_f, \quad z(t_f) = z_f. \end{aligned} \tag{5}$$

2.1.2 Optimal control of the reentry trajectory

Due to dynamic constraints, boundary constraints and path constraints, the aim of the reentry trajectory optimization problem is to determine the control $\bar{U}$ that minimizes the objective function. Therefore, the performance

index of the reentry trajectory can be defined

$$J = \Theta[X(t_f)] + \int_{t_0}^{t_f} [k_n \dot{Q}_n(t) + k_1 q(t) + k_2 n(t)]dt,$$
$$\Theta[X(t_f)] = k_3(V_f - V)^2 + k_4(x_f - x)^2 + k_5(z_f - z)^2, \quad (6)$$

where $\dot{Q}_n$ is the heating rate of each part on the surface of reentry vehicle; q is the dynamic pressure; n is the aerodynamic load; t_0 and t_f are the initial time and final time, respectively; k_n, k_1, k_2, k_3, k_4 and k_5 are the weight coefficients; V_f, x_f and z_f are the terminal velocity, transverse and lateral distance.

The initial conditions can be written

$$\mathbf{X}(t_0) = \mathbf{X}_0, \ \ \mathbf{U} \in \Omega, \ \ t \in [t_0, t_f], \quad (7)$$

where Ω is the bounded closed set.

The terminal constraints can be written

$$\bar{\mathbf{M}}[\mathbf{X}(t_f), t_f] = \mathbf{0}. \quad (8)$$

The Hamilton function is introduced as

$$H = k_n \dot{\bar{Q}}_n(t) + k_1 q(t) + k_2 n(t) + \boldsymbol{\lambda}^{\mathrm{T}} \mathbf{f}(\mathbf{X}, \bar{\mathbf{U}}, t), \quad (9)$$

where $\boldsymbol{\lambda}(t)$ is the Lagrange multiplier vector.

The necessary conditions of optimal control can be written

$$\dot{\mathbf{X}} = \frac{\partial H}{\partial \boldsymbol{\lambda}}, \ \ \bar{\mathbf{U}} = \arg\sup_{\bar{\mathbf{U}} \in \Omega} H,$$
$$\dot{\boldsymbol{\lambda}} = -\frac{\partial H}{\partial \mathbf{X}}, \ \ \boldsymbol{\lambda}(t_f) = \frac{\partial \Theta[\mathbf{X}(t_f), t_f]}{\partial \mathbf{X}}, \quad (10)$$

where arg is the inverse function.

By using the conjugate gradient method in the optimal control theory, the optimal trajectory and flight control variables can be obtained.

2.2. Optimization results

The optimal trajectory of reentry vehicle is simulated numerically herein. The initial conditions of reentry trajectory optimization are taken as: the altitude of the reentry point is 120 km, the reentry velocity is 7.8 km/s, and the reentry angle is $-3.74°$. Under the same reentry altitude and velocity, reentry angle obviously influences the aerodynamic heating rate and aerodynamic overload undertaken by the reentry vehicle, as well as its flight distance in the atmosphere. Fig. 1 shows the relationship among reentry angle, heating rate and transverse distance. As shown in Fig. 1, the smaller the reentry angle is, the smaller the aerodynamic heating rate is, and the longer the flight distance is. However, if the reentry angle is too small, reentry flight of the vehicle may fail because the reentry vehicle is bounced out of the atmosphere. If the reentry angle is too large, the flight times minimum, resulting in the shortening of flying distance and the lessening of total aerodynamic heating of the vehicle, while transient aerodynamic heating rate may be suddenly increased causing the damage of the vehicle. Therefore, the reentry angle shall be controlled within a proper range. As shown in Fig. 1, if the absolute value of reentry angle is larger than 3.8°, the heating rate will be beyond the constraint condition $\dot{\bar{Q}}_n \leq \dot{\bar{Q}}_{n\max} = 420$ kW/m^2; and if the absolute value of reentry angle is smaller than 3.6°, the transverse distance may not satisfy the constraint condition $x \leq 3500$ km. Under the constraint conditions of heating rate and transverse distance, the reentry angle may be optimized to be $-3.74°$.

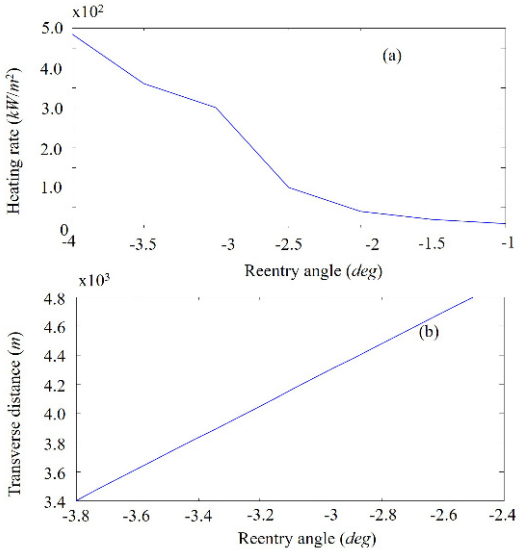

Fig. 1. Changes of heating rate and transverse distance of the reentry vehicle varying with reentry angle: (a) heating rate, (b) transverse distance.

The reentry trajectory of the reentry vehicle is shown in Fig. 2. Figure 3 shows the time histories of temperature, heating rate and overload of the vehicle. It can be observed from Figs. 2-3 that, under the reentry angle $-3.74°$, the constraint conditions given in Section 2.1.1 are satisfied, and the aerodynamic heating rate on the surface of the reentry vehicle is significantly decreased.

3. FLUTTER MODEL OF TWO-DIMENSIONAL WING

In the flight of reentry vehicle, aerodynamic load on some parts of the vehicle is still very large at some moment of reentry flight, this may cause the wing to flutter. In this section, flutter problem for a two-dimensional wing including cubic hard spring nonlinearity is analyzed. We can observe from Fig. 3 that the aerodynamic heating rate and temperature of the reentry vehicle may be reduced sig-

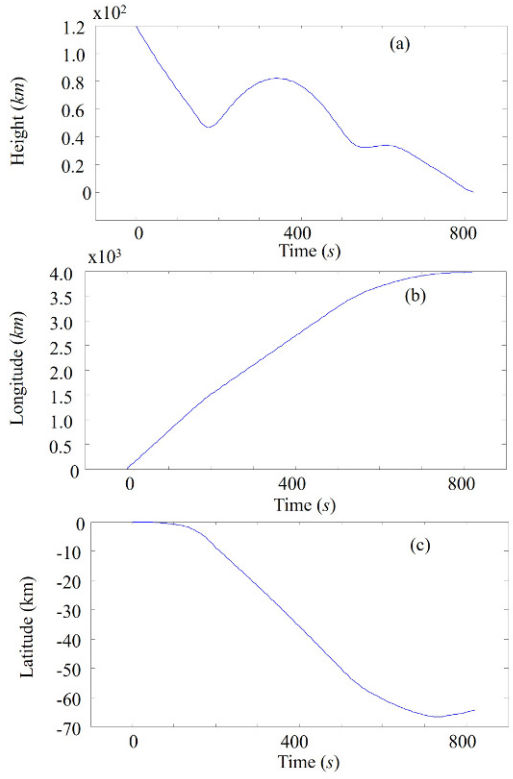

Fig. 2. Reentry trajectory of the reentry vehicle: (a) Height, (b) longitude, (c) latitude.

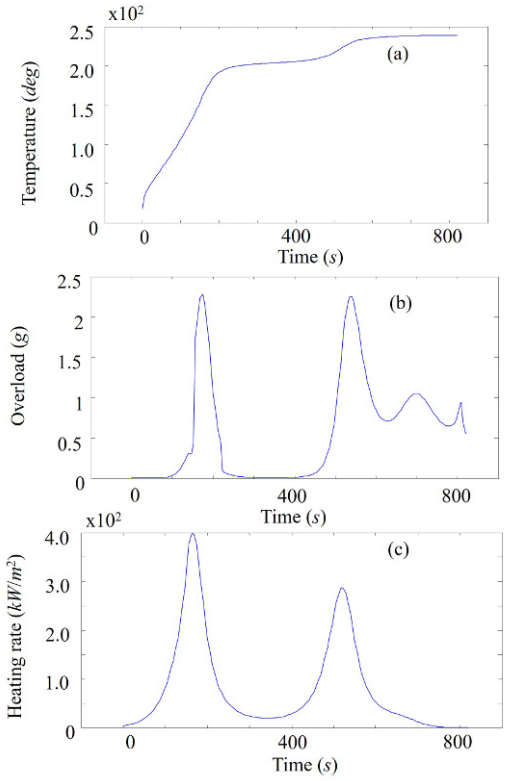

Fig. 3. Time histories of temperature, overload and heating rate of the reentry vehicle: (a) temperature, (b) overload, (c) heating rate.

nificantly after the appropriate trajectory optimization. As a result, the influence of temperature on wing flutter may be ignored.

As shown in Fig. 4, a two degree-of-freedom (2-dof) wing system model is considered herein. The plunge deflection is denoted by h, positive in the downward direction; θ is the pitch angle about the elastic axis, positive nose up; the chord length is c; Q, p and C are the aerodynamic center, elastic axis and center of mass, respectively; δ_{LEout} and δ_{LEin} (or δ_{REout} and δ_{REin}) are the control surface angles.

From Fig. 4, the velocity of mass center of wing can be expressed as

$$\dot{z} = \dot{h} + (x_C - x_p)\dot{\theta}. \tag{11}$$

The kinetic energy, potential energy and dissipation of the system can be given by

$$\begin{aligned} T &= \frac{1}{2}m_W\dot{z}^2 + \frac{1}{2}m_e\dot{h}^2 + \frac{1}{2}I_C\dot{\theta}^2, \\ U &= \frac{1}{2}K_h h^2 + \frac{1}{2}K_\theta\theta^2, \quad \zeta = \frac{1}{2}C_h\dot{h}^2 + \frac{1}{2}C_\theta\dot{\theta}^2, \end{aligned} \tag{12}$$

where I_C, m_W, m_e, K_h, K_θ, C_h and C_θ are the moment of inertia about center of mass, wing mass, wing extra-mass, stiffness coefficient in plunge, torsion stiffness coefficient,

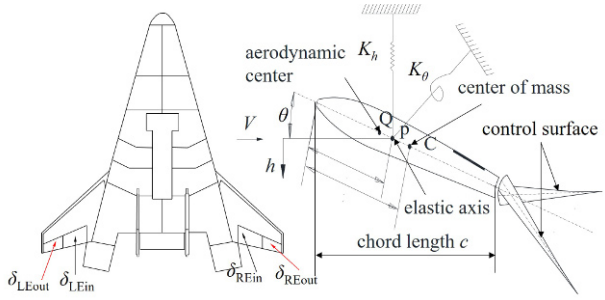

Fig. 4. Two-dimensional airfoil model with control surface.

damping coefficient in plunge and torsion damping coefficient, respectively.

For supersonic and hypersonic flow, the piston theory is widely used to calculate the aerodynamics acting on a lifting surface [24]. Applying the piston theory, the aerodynamic force and moment acting on the wing can be obtained as

$$\begin{aligned} L = \frac{2\rho_1 V\bar{\gamma}c}{M_\infty}&[0.5c(1-x_0)\dot{\theta} + \dot{h} + V\theta \\ &+ \frac{1}{12}V\bar{\gamma}^2(\kappa+1)M_\infty^2\theta^3], \end{aligned}$$

$$T=\frac{\rho_1 V\bar{\gamma}c^2}{M_\infty}[\frac{1}{6}c(4-6x_0+3x_0^2)\dot{\theta}+(1-x_0)\dot{h} \quad (13)$$
$$+V(1-x_0)\theta+\frac{1}{12}\bar{\gamma}^2(\kappa+1)M_\infty^2(1-x_0)V\theta^3],$$

where M_∞ is the Mach number; $\bar{\gamma}$ is the aerodynamic correction factor, $\bar{\gamma}=M_\infty/\sqrt{M_\infty^2-1}$; κ is the the ratio of specific heat; x_0 is the non-dimensional distance from the leading edge to the elastic axis.

The aerodynamic lift and moment caused by control surface can be expressed as

$$L_{\delta_{LEout}}=L_{\delta_{LEin}}=\frac{1}{2}\rho_1 V^2 c a_C s_\beta \delta_{LEout},$$
$$M_{\delta_{LEout}}=M_{L_{\delta_{LEin}}}=\frac{1}{2}\rho_1 V^2 c^2 b_C s_\beta \delta_{LEout}, \quad (14)$$

where a_C is the coefficients of lift force, b_C is the ratio of the pitching moment M to the deflection angle, and s_β is the span of control surface.

The moment caused by the cubic hard spring nonlinearity of the wing can be written as [25].

$$M(\theta)=K_\theta\theta+e_{n1}\theta^3, \quad (15)$$

where e_{n1} is the nonlinear stiffness coefficient.

Without considering structural damping, the aeroelastic equation of the two-dimensional wing system can be deduced using the Lagrangian method, given by

$$\tilde{\mathbf{A}}\ddot{\mathbf{q}}(t)+\rho V\tilde{\mathbf{B}}\dot{\mathbf{q}}(t)+(\rho V^2\tilde{\mathbf{C}}+\tilde{\mathbf{D}})\mathbf{q}(t)+\tilde{\mathbf{f}}(t)=\tilde{\mathbf{b}}\mathbf{u}(t) \quad (16)$$

where $\mathbf{q}(t)=[\ h(t)\quad \theta(t)\ ]^{\mathrm{T}}$ is the generalized displacement vector; and $\tilde{\mathbf{A}}$, $\tilde{\mathbf{B}}$, $\tilde{\mathbf{C}}$ and $\tilde{\mathbf{D}}$ are the inertia, aerodynamic damping, aerodynamic stiffness and structural stiffness matrices, respectively; and $\mathbf{u}(t)=[\delta_{LEout},\ \delta_{LEin}]^{\mathrm{T}}$ is the control input. The expressions of parameters in (16) are

$$\tilde{\mathbf{A}}=\begin{bmatrix} \frac{mS^3c}{3} & \frac{mS^2}{2}(\frac{c^2}{2}-cx_f) \\ \frac{mS^2}{2}(\frac{c^2}{2}-cx_f) & mS(\frac{c^3}{3}-c^2x_f+cx_f^2)\end{bmatrix},$$
$$\tilde{\mathbf{C}}=\begin{bmatrix} 0 & \frac{2\bar{\gamma}c}{M_\infty} \\ 0 & -\frac{\bar{\gamma}c^2}{M_\infty}(1-x_0)\end{bmatrix},\quad \tilde{\mathbf{D}}=\begin{bmatrix} K_h & 0 \\ 0 & K_\theta\end{bmatrix},$$
$$\tilde{\mathbf{B}}=\begin{bmatrix} -\frac{2\bar{\gamma}c}{M_\infty} & -\frac{\bar{\gamma}c^2}{M_\infty}(1-x_0) \\ \frac{\bar{\gamma}c^2}{M_\infty}(1-x_0) & \frac{\bar{\gamma}c^3}{6M_\infty}(4-6x_0+3x_0^2)\end{bmatrix},$$
$$\tilde{\mathbf{f}}=\begin{bmatrix} -\frac{1}{6}\rho_1 V^2\bar{\gamma}^3 c(\kappa+1)M_\infty\theta^3 \\ \frac{1}{12}\rho_1 V^2\bar{\gamma}^3c^2(\kappa+1)M_\infty(1-x_0)\theta^3+e_{n1}\theta^3\end{bmatrix}.$$

Equation (16) can be further changed to be

$$\dot{\mathbf{x}}(t)=\mathbf{A}\mathbf{x}(t)+\mathbf{B}\mathbf{u}(t)+\mathbf{f}(t) \quad (17)$$

where $\mathbf{x}=[h(t),\ \theta(t),\ \dot{h}(t),\ \dot{\theta}(t)]^{\mathrm{T}}$ is the state space vector; $\mathbf{A}=\begin{bmatrix} \mathbf{0} & \mathbf{I} \\ -\tilde{\mathbf{A}}^{-1}(\rho_1V^2\tilde{\mathbf{C}}+\tilde{\mathbf{D}}_1) & -\tilde{\mathbf{A}}^{-1}\rho_1V\tilde{\mathbf{B}}\end{bmatrix}$, $\mathbf{B}=\begin{bmatrix} \mathbf{0} \\ \tilde{\mathbf{A}}^{-1}\tilde{\mathbf{b}}\end{bmatrix}$ and $\mathbf{f}=\begin{bmatrix} \mathbf{0} \\ -\tilde{\mathbf{A}}^{-1}\tilde{\mathbf{f}}(t)\end{bmatrix}$. The parameters in the matrices $\mathbf{A}$ and $\mathbf{B}$ are determined based on the computing results for the most serious moment of reentry flight of the vehicle given in Section 2.3. In this serious moment, the flight velocity of the vehicle is maximum and the aerodynamic load on the wing surface is maximum too. From the computing results in Section 2.2, the reentry will reach its maximum velocity of 1406 m/s at the moment 699.19 s; the altitude, longitude, latitude and atmospheric density of the reentry vehicle at this serious moment can be determined to be 21.87 km, 3907.11 km, −66.05 km, and 0.0644 kg/m^3, respectively.

4. FINITE-TIME H_∞ ADAPTIVE FAULT-TOLERANT CONTROL DESIGN

Note that the dynamic equation of flutter in (17), assumes that all of the actuators are fault-free, and it is called the nominal flutter system. For an active flutter control system, it is difficult to ensure the actuator in the ideal working condition. They are likely to have some problems, such as loss of effectiveness and float. Therefore, fault tolerance capability should be considered in flutter controller design.

Now, we consider two types of actuator fault simultaneously, namely the float fault and the loss of effectiveness of the actuators as well as actuator saturation, parameter uncertainties and external disturbances. Hence, the flutter dynamic model given by (17) can be rewritten as

$$\begin{cases} \dot{\mathbf{x}}(t)=[\mathbf{A}+\Delta\mathbf{A}(t)]\mathbf{x}(t)+(\mathbf{B}+\Delta\mathbf{B})\boldsymbol{\rho}\mathbf{v} \\ \quad +(\mathbf{B}+\Delta\mathbf{B})\mathbf{u}_s(t)+\mathbf{f}(t,\mathbf{x})+\mathbf{B}_1\mathbf{w}(t) \\ \mathbf{y}(t)=\mathbf{c}_1\mathbf{x}(t),\end{cases} \quad (18)$$

where $\Delta\mathbf{A}$ represents the time-varying parameter uncertainties; $\Delta\mathbf{B}$ stands for the input uncertainties; $\boldsymbol{\rho}=diag(\rho_1,\ \rho_2)$ denotes the effectiveness factor matrix for actuators with $0<\rho_i\le 1\ (i=1,\ 2)$; The case when $\rho_i=1$ means that the i-th actuator works normally, and $0<\rho_i<1$ denote the case in which the i-th actuator partially loses its effectiveness; $\mathbf{u}_s(t)=(u_{s1},\ u_{s2})\in\Re^{2\times1}$ corresponds to the case in which the i-th actuator float fault of flutter system; $\mathbf{u}(t)$ is the control signal to be designed, and $\mathbf{v}$ denotes the saturation function; $\mathbf{f}(t,\mathbf{x})$ denotes the nonlinear term arouse by the cubic structure nonlinearity and the nonlinearity of the generalized aerodynamic force and moment in the flutter system; $\mathbf{w}(t)$ represents the bounded external disturbances; and $\mathbf{y}(t)$ is the measured output. The parameters $\mathbf{B}_1$ and $\mathbf{c}_1$ are known matrices with appropriate dimensions. $\Delta\mathbf{A}$ and $\Delta\mathbf{B}$ are assumed to satisfy the following matching condition

$$\mathbf{B}_1=\mathbf{B}\mathbf{F},\ \ \Delta\mathbf{A}=\mathbf{B}\mathbf{N}(t),\ \ \Delta\mathbf{B}=\mathbf{M}\mathbf{B}, \quad (19)$$
$$\left\|\mathbf{x}^{\mathrm{T}}(t)\tilde{\mathbf{P}}^j\Delta\mathbf{B}\right\|\le\theta_1\left\|\mathbf{x}^{\mathrm{T}}(t)\tilde{\mathbf{P}}^j\mathbf{B}\right\|, \quad (20)$$

where $\mathbf{F}$ and $\mathbf{M}$ are both known matrices; $\|\cdot\|$ represents Euclidean norm of vectors or matrices; $\mathbf{N}(t)$ is an unknown matrix with $\|\mathbf{N}\| \le l^*$, l^* is an unknown constant; and θ_1 is any positive constant.

$\mathbf{v}$ is a saturation function defined as

$$\mathbf{v} = \begin{cases} \mathbf{v}_{\max}, & \mathbf{u}(t) > \mathbf{v}_{\max} \\ \mathbf{u}(t) + \boldsymbol{\delta}_{\mathbf{u}}(\mathbf{x}), & |\mathbf{u}(t)| \le \mathbf{v}_{\max} \\ -\mathbf{v}_{\max}, & \mathbf{u}(t) < -\mathbf{v}_{\max}, \end{cases} \tag{21}$$

where $\mathbf{v}_{\max}$ and $\boldsymbol{\delta}_{\mathbf{u}}(\mathbf{x})$ are the actuator saturation level and auxiliary variable.

In nonlinear control problem, the radial basis function (RBF) network is usually used as a tool for modeling nonlinear system because of its good capabilities in function approximation. In this paper, the unknown $\boldsymbol{\delta}_{\mathbf{u}}(\mathbf{x})$ is approximated by the RBF network [26]

$$\begin{aligned} h_N(\bar{\mathbf{x}}) &= \exp(-\frac{\|\bar{\mathbf{x}} - \mathbf{c}_N\|^2}{2b_N^2}), \\ \boldsymbol{\delta}_{\mathbf{u}}(\mathbf{x}) &= \mathbf{W}^{*\mathrm{T}}\mathbf{h}(\mathbf{x}) + \boldsymbol{\varepsilon}_{\mathbf{u}}(\mathbf{x}),\ \mathbf{x} \in \mathbf{D}_{\mathbf{x}}, \end{aligned} \tag{22}$$

where $\bar{\mathbf{x}}$ is the input of neural networks; $h_N(\mathbf{x})$ is the Gaussian function vector; $\mathbf{c}_N$ and b_N are the centre vector and width; $\mathbf{W}^*$ is the ideal weight matrix; $\boldsymbol{\delta}_{\mathbf{u}}(\mathbf{x})$ is the output of neural networks; $\hat{\boldsymbol{\delta}}_{\mathbf{u}}(\mathbf{x}) = \hat{\mathbf{W}}^{\mathrm{T}}\mathbf{h}(\mathbf{x})$ denotes the estimate of $\boldsymbol{\delta}_{\mathbf{u}}(\mathbf{x})$, $\tilde{\boldsymbol{\delta}}_{\mathbf{u}}(\mathbf{x}) = \boldsymbol{\delta}_{\mathbf{u}}(\mathbf{x}) - \hat{\boldsymbol{\delta}}_{\mathbf{u}}(\mathbf{x})$; $\hat{\mathbf{W}}$ denotes the estimate of $\mathbf{W}^*$; $\boldsymbol{\varepsilon}_{\mathbf{u}}(\mathbf{x})$ is the approximation error; and $\mathbf{D}_{\mathbf{x}}$ is a sufficiently large compact set $\mathbf{D}_{\mathbf{x}} \in \Re^{4\times 1}$.

Using (18) to design controller, we have

$$\mathbf{u}(t) = [\hat{\mathbf{K}}_1(t) + \mathbf{K}_2(t) + \mathbf{K}_3(t)]\mathbf{x}(t) - \hat{\boldsymbol{\delta}}_{\mathbf{u}}(\mathbf{x}), \tag{23}$$

where $\hat{\mathbf{K}}_1(t)$ is given by an adaptive function for guarantee the stability of the system; $\mathbf{K}_2(t)$ and $\mathbf{K}_3(t)$ are by an adaptive function for eliminating the effects of bounded unparametrizable stuck, external disturbances and parameter uncertainties. The expressions of $\hat{\mathbf{K}}_1(t)$, $\mathbf{K}_2(t)$ and $\mathbf{K}_3(t)$ are given below. We can prove that these expressions may guarantee the stability of the control system. The proof procedure is given in the sequel.

In the flight of reentry vehicle, sensor fault is one of the most important problems which usually appears in many wing flutter control systems. Considering sensor fault, the controller is designed as

$$\mathbf{u}(t) = [\hat{\mathbf{K}}_1(t) + \mathbf{K}_2(t) + \mathbf{K}_3(t)]\mathbf{G}\mathbf{x}(t) - \hat{\boldsymbol{\delta}}_{\mathbf{u}}(\mathbf{x}), \tag{24}$$

where $\mathbf{G} = diag(G_1,\ G_2,\ G_3,\ G_4)$. $G_i = 0$ represents the total loss of effectiveness of sensor of the i-th state, $0 < G_i < 1$ the partial loss of effectiveness and $G_i = 1$ the normal.

Below we give the expressions of $\hat{\mathbf{K}}_1(t)$, $\mathbf{K}_2(t)$ and $\mathbf{K}_3(t)$ and then utilize the Lyapunov method to prove that the controller given by (23) can guarantee the stability of the system. The adaptive gain $\hat{\mathbf{K}}_{1i}(t)$ is chosen as

$$\frac{d\hat{\mathbf{K}}_{1i}(t)}{dt} = -\Gamma_i \mathbf{G}\mathbf{x}(t)\mathbf{x}^{\mathrm{T}}(t)\bar{\tilde{\mathbf{P}}}^j(\mathbf{I}+\mathbf{M})\mathbf{b}_i, \quad i = 1,\ 2, \tag{25}$$

where Γ_i is any positive constant; $\mathbf{I}$ denotes the identity matrix with an appropriate dimension and $\mathbf{b}_i$ is the i-th column of B; $\tilde{\mathbf{P}}^j$ denotes the each faulty mode has its corresponding positive-definite matrix $\mathbf{P}$, where j denotes the j-th faulty mode; $\bar{\tilde{\mathbf{P}}}^j$ denotes the maximum norm of the $\tilde{\mathbf{P}}^j$, namely $\bar{\tilde{\mathbf{P}}}^j := \{\tilde{\mathbf{P}}^j :\ \max_j(\|\tilde{\mathbf{P}}^j\|)\}$.

$\mathbf{K}_2(t)$ and $\mathbf{K}_3(t)$ are given as

$$\mathbf{K}_2(t) = \frac{\mathbf{B}^{\mathrm{T}}\bar{\tilde{\mathbf{P}}}^j\beta_1 \left\|\mathbf{x}^{\mathrm{T}}(t)\bar{\tilde{\mathbf{P}}}^j\mathbf{B}\right\| \hat{k}_4(t)}{\alpha_1 \left\|\mathbf{x}^{\mathrm{T}}(t)\bar{\tilde{\mathbf{P}}}^j\mathbf{B}\right\|^2}, \tag{26}$$

$$\mathbf{K}_3(t) = \frac{1}{2}\eta\mathbf{B}^{\mathrm{T}}\bar{\tilde{\mathbf{P}}}^j\hat{k}_5(t), \tag{27}$$

where $\hat{k}_4$ and $\hat{k}_5$ are updated by the following adaptive equations

$$\frac{d\hat{k}_4(t)}{dt} = -r_1(1+\theta_1)\left\|\mathbf{x}^{\mathrm{T}}(t)\bar{\tilde{\mathbf{P}}}^j\mathbf{B}\right\|, \tag{28}$$

$$\frac{d\hat{k}_5(t)}{dt} = -r_2\eta(1+\theta_1)\left\|\mathbf{x}^{\mathrm{T}}(t)\bar{\tilde{\mathbf{P}}}^j\mathbf{B}\right\|^2. \tag{29}$$

The weight matrix $\hat{\mathbf{W}}$ is updated by the following adaptive equations

$$\frac{d\hat{\mathbf{W}}}{dt} = r_3\mathbf{h}(\mathbf{x})\mathbf{x}^{\mathrm{T}}(t)\bar{\tilde{\mathbf{P}}}^j(\mathbf{I}+\mathbf{M})\mathbf{b}_i, \quad i = 1,\ 2. \tag{30}$$

Denote

$$\tilde{\mathbf{K}}_1(t) = \mathbf{K}_1 - \hat{\mathbf{K}}_1(t), \tag{31}$$

$$\tilde{k}_4(t) = k_4 - \hat{k}_4(t), \tag{32}$$

$$\tilde{k}_5(t) = k_5 - \hat{k}_5(t), \tag{33}$$

$$\tilde{\mathbf{W}}^{\mathrm{T}} = \mathbf{W}^{*\mathrm{T}} - \hat{\mathbf{W}}^{\mathrm{T}}. \tag{34}$$

Substituting (21), (24) into (18), we have

$$\begin{cases} \dot{x}(t) = [A + \Delta A(t)]x(t) + (B + \Delta B)\rho[(\hat{K}_1(t) \\ \qquad + K_2(t) + K_3(t))Gx(t) - \hat{\delta}_u(x) + \delta_u(x)] \\ \qquad + (B + \Delta B)u_s(t) + f(t,\ x) + B_1 w(t) \\ y(t) = c_1 x(t). \end{cases} \tag{35}$$

Assumption 1: For any given positive number d_s, d_f, d_w, d_δ and the actual working time T_f, the stuck $\mathbf{u}_s(t)$, nonlinear vector field $\mathbf{f}(t,\mathbf{x})$, external disturbances $\mathbf{w}(t)$,

and $\bar{\delta}_{\mathbf{u}}(\mathbf{x})$ are time-varying and satisfies

$$\begin{cases} \int_0^{T_f} \mathbf{u}_s^{\mathrm{T}}(t)\mathbf{u}_s(t)dt \le d_s, \quad d_s \ge 0 \\ \int_0^{T_f} \mathbf{f}^{\mathrm{T}}(t,\mathbf{x})\mathbf{f}(t,\mathbf{x})dt \le d_f, \quad d_f \ge 0 \\ \int_0^{T_f} \mathbf{w}^{T}(t)\mathbf{w}(t)dt \le d_w, \quad d_w \ge 0 \\ \int_0^{T_f} \bar{\delta}_{\mathbf{u}}^{T}(\mathbf{x})\bar{\delta}_{\mathbf{u}}(\mathbf{x})dt \le d_{\delta}, \quad d_{\delta} \ge 0. \end{cases} \tag{36}$$

Assumption 2: For any $x(t)$, there exists positive constants μ, α_1, β_1 and k_4, such that

$$\left\|\mathbf{x}^{\mathrm{T}}(t)\tilde{\mathbf{P}}^j\mathbf{B}\rho\mathbf{B}^{\mathrm{T}}\bar{\tilde{\mathbf{P}}}^j\mathbf{G}\mathbf{x}(t)\right\| \le \mu\left\|\mathbf{x}^{\mathrm{T}}(t)\bar{\tilde{\mathbf{P}}}^j\mathbf{B}\right\|^2, \tag{37}$$

$$\alpha_1\left\|\mathbf{x}^{\mathrm{T}}(t)\bar{\tilde{\mathbf{P}}}^j\mathbf{B}\right\|^2 \ge \beta_1\left\|\mathbf{x}^{\mathrm{T}}(t)\sqrt{\mathbf{G}}\bar{\tilde{\mathbf{P}}}^j\mathbf{B}\sqrt{\rho}\right\|^2, \tag{38}$$

$$\begin{aligned}&\left\|\mathbf{x}^{\mathrm{T}}(t)\bar{\tilde{\mathbf{P}}}^j\mathbf{B}\right\|k_4 + \left\|\mathbf{x}^{\mathrm{T}}(t)\tilde{\mathbf{P}}^j\mathbf{B}\right\|\|\mathbf{u}_s(t)\| \\ &\quad + \left\|\mathbf{x}^{\mathrm{T}}(t)\tilde{\mathbf{P}}^j\mathbf{B}\right\|\|\rho\|\varepsilon_{\mathbf{u}\max} + \left\|\mathbf{x}^{\mathrm{T}}(t)\tilde{\mathbf{P}}^j\mathbf{B}\right\|\|\mathbf{F}\|d_w \le 0.\end{aligned} \tag{39}$$

Moreover, k_5 is a constant satisfying

$$k_5 = \frac{l^{*2}}{-(1+\theta_1)\mu}. \tag{40}$$

Definition 1 [27] (Finite-Time Bounded, FTB)**:** For given positive constants c_1, d_s, d_f, d_w, d_δ, T_f, and a symmetric matrix $\mathbf{R} > 0$, the resulting closed-loop system (35) is said to be robustly FTB with respect to (c_1, c_2, T_f, $\mathbf{R}$, d_s, d_f, d_w, d_δ), if there exists a constant $c_2 (> c_1)$, such that

$$\mathbf{x}_0^{\mathrm{T}}\mathbf{R}\mathbf{x}_0 \le c_1 \Rightarrow \mathbf{x}^{\mathrm{T}}(t)\mathbf{R}\mathbf{x}(t) < c_2, \quad \forall t \in [0 \ \ T_f] \tag{41}$$

Definition 2 [28]**:** If there exists state feedback controller in form (24), such that the resulting closed-loop system (35) is FTB with respect to (c_1, c_2, T_f, $\mathbf{R}$, d_s, d_f, d_w, d_δ) and under the assumed zero initial condition, the system output satisfies the following inequality for $T_f > 0$ and for all admissible $\mathbf{w}(t)$ which satisfy Assumption 1:

$$\int_0^{T_f} \mathbf{y}^{\mathrm{T}}(t)\mathbf{y}(t)dt \le \gamma^2 \int_0^{T_f} \mathbf{w}^{T}(t)\mathbf{w}(t)dt. \tag{42}$$

Then the state feedback controller (24) is called as the robust finite-time H_∞ controller of the nonlinear systems (35).

Lemma 1 [29] (The Schur complement lemma)**:** For given symmetric matrix $\mathbf{S} = \begin{bmatrix} \mathbf{S}_{11} & \mathbf{S}_{12} \\ \mathbf{S}_{21} & \mathbf{S}_{22} \end{bmatrix}$, the following three conditions are equivalent

$$\begin{cases} (1) \quad S < 0, \\ (2) \quad S_{11} < 0, \quad S_{22} - S_{12}^{\mathrm{T}}S_{11}^{-1}S_{12} < 0, \\ (3) \quad S_{22} < 0, \quad S_{11} - S_{12}S_{22}^{-1}S_{12}^{\mathrm{T}} < 0. \end{cases} \tag{43}$$

Theorem 1: For given positive constants α_0, c_1, T_f, d_s, d_f, d_w, d_δ and a symmetric matrix $\mathbf{R} > 0$, the closed-loop controlled system (35) is FTB with respect to (c_1, c_2, T_f, $\mathbf{R}$, d_s, d_f, d_w, d_δ), if there exist positive constant c_2 and symmetric positive-definite matrix $\tilde{\mathbf{P}}$, such that

$$\begin{bmatrix} \mathbf{\Omega} & \tilde{\mathbf{P}}^j(\mathbf{B}+\Delta\mathbf{B})\rho & \tilde{\mathbf{P}}^j(\mathbf{B}+\Delta\mathbf{B}) & \tilde{\mathbf{P}}^j & \tilde{\mathbf{P}}^j\mathbf{B}_1 \\ * & -\mathbf{I} & 0 & 0 & 0 \\ * & * & -\mathbf{I} & 0 & 0 \\ * & * & * & -\mathbf{I} & 0 \\ * & * & * & * & -\mathbf{I} \end{bmatrix} < 0, \tag{44}$$

$$\frac{c_1}{\lambda_{\min}(\mathbf{P}^j)} + (d_s + d_f + d_w + d_\delta) < \frac{c_2 e^{-\alpha_0 t}}{\lambda_{\max}(\mathbf{P}^j)}, \tag{45}$$

where $\mathbf{\Omega} = \tilde{\mathbf{P}}^j\bar{\mathbf{A}} + \bar{\mathbf{A}}^{\mathrm{T}}\tilde{\mathbf{P}}^j - \alpha_0\tilde{\mathbf{P}}^j$, $\tilde{\mathbf{P}}^j = \mathbf{R}^{\frac{1}{2}}\mathbf{P}^j\mathbf{R}^{\frac{1}{2}}$ and $\bar{\mathbf{A}} = \mathbf{A} + \Delta\mathbf{A}(t) + (\mathbf{B}+\Delta\mathbf{B})\rho[\hat{\mathbf{K}}_1(t) + \mathbf{K}_2(t) + \mathbf{K}_3(t)]\mathbf{G}$.

Proof: For the closed-loop system (35), we first define a Lyapunov functional candidate as $V(\mathbf{x}(t)) = \mathbf{x}^{\mathrm{T}}(t)\tilde{\mathbf{P}}^j\mathbf{x}(t)$. Then

$$\begin{aligned}\dot{V}(\mathbf{x}(t)) =& \dot{\mathbf{x}}^{\mathrm{T}}(t)\tilde{\mathbf{P}}^j\mathbf{x}(t) + \mathbf{x}^{\mathrm{T}}(t)\tilde{\mathbf{P}}^j\dot{\mathbf{x}}(t) \\ =& \mathbf{x}^{\mathrm{T}}(t)[\tilde{\mathbf{P}}^j\bar{\mathbf{A}} + \bar{\mathbf{A}}^{\mathrm{T}}\tilde{\mathbf{P}}^j]\mathbf{x}(t) \\ &+ 2\mathbf{x}^{\mathrm{T}}(t)\tilde{\mathbf{P}}^j(\mathbf{B}+\Delta\mathbf{B})\rho\bar{\delta}_{\mathbf{u}}(\mathbf{x}) \\ &+ 2\mathbf{x}^{\mathrm{T}}(t)\tilde{\mathbf{P}}^j(\mathbf{B}+\Delta\mathbf{B})\mathbf{u}_s(t) \\ &+ 2\mathbf{x}^{\mathrm{T}}(t)\tilde{\mathbf{P}}^j\mathbf{f}(t,\mathbf{x}) + 2\mathbf{x}^{\mathrm{T}}(t)\tilde{\mathbf{P}}^j\mathbf{B}_1\mathbf{w}(t).\end{aligned} \tag{46}$$

Define the following function

$$\begin{aligned}J_1 =& \dot{V}(\mathbf{x}(t)) - \alpha_0\mathbf{x}^{\mathrm{T}}(t)\tilde{\mathbf{P}}^j\mathbf{x}(t) - \bar{\delta}_{\mathbf{u}}^{\mathrm{T}}(\mathbf{x})\bar{\delta}_{\mathbf{u}}(\mathbf{x}) \\ &- \mathbf{u}_s^{\mathrm{T}}(t)\mathbf{u}_s(t) - \mathbf{f}^{\mathrm{T}}(t,\mathbf{x})\mathbf{f}(t,\mathbf{x}) - \mathbf{w}^{\mathrm{T}}(t)\mathbf{w}(t).\end{aligned} \tag{47}$$

The condition inequality (44) implies $J_1 < 0$. Multiplying the above inequality by $e^{-\alpha_0 t}$, we derive

$$\begin{aligned}\frac{d}{dt}(e^{-\alpha_0 t}V(\mathbf{x}(t))) <& e^{-\alpha_0 t}(\bar{\delta}_{\mathbf{u}}^{\mathrm{T}}(\mathbf{x})\bar{\delta}_{\mathbf{u}}(\mathbf{x}) \\ &+ \mathbf{u}_s^{\mathrm{T}}(t)\mathbf{u}_s(t) + \mathbf{f}^{\mathrm{T}}(t,\mathbf{x})\mathbf{f}(t,\mathbf{x}) \\ &+ \mathbf{w}^{\mathrm{T}}(t)\mathbf{w}(t)).\end{aligned} \tag{48}$$

Note that $\tilde{\mathbf{P}}^j = \mathbf{R}^{\frac{1}{2}}\mathbf{P}^j\mathbf{R}^{\frac{1}{2}}$. By integrating the aforementioned inequality between 0 and t, we get

$$\begin{aligned}V(\mathbf{x}(t)) <& e^{\alpha_0 t}V(\mathbf{x}_0) + e^{\alpha_0 t}\int_0^t e^{-\alpha_0 t_0}(\bar{\delta}_{\mathbf{u}}^{\mathrm{T}}(\mathbf{x})\bar{\delta}_{\mathbf{u}}(\mathbf{x}))dt_0 \\ &+ e^{\alpha_0 t}\int_0^t e^{-\alpha_0 t_0}(\mathbf{u}_s^{\mathrm{T}}(t)\mathbf{u}_s(t) + \mathbf{f}^{\mathrm{T}}(t,\mathbf{x})\mathbf{f}(t,\mathbf{x}) \\ &+ \mathbf{w}^{\mathrm{T}}(t)\mathbf{w}(t))dt_0 \\ \le& \lambda_{\max}(\mathbf{P}^j)c_1e^{\alpha_0 t} + (d_s + d_f + d_w)e^{\alpha_0 t}.\end{aligned} \tag{49}$$

On the other hand, the following condition holds:

$$V(\mathbf{x}(t)) = \mathbf{x}^{\mathrm{T}}(t)\mathbf{R}^{\frac{1}{2}}\mathbf{P}^j\mathbf{R}^{\frac{1}{2}}\mathbf{x}(t) \ge \lambda_{\min}(\mathbf{P}^j)\mathbf{x}^{\mathrm{T}}(t)\mathbf{R}\mathbf{x}(t). \tag{50}$$

From (49) and (50), we can get

$$\mathbf{x}^{\mathrm{T}}(t)\mathbf{R}\mathbf{x}(t) < \frac{\lambda_{\max}(\mathbf{P}^j)c_1 e^{\alpha_0 t} + (d_s + d_f + d_w + d_\delta)e^{\alpha_0 t}}{\lambda_{\min}(\mathbf{P}^j)}. \tag{51}$$

Condition (45) implies that for $\forall t \in [0 \quad T_f]$, $\mathbf{x}^{\mathrm{T}}(t)\mathbf{R}\mathbf{x}(t) < c_2$. According to Definition 1, this completes the proof. □

Theorem 2: For given positive constants α_0, c_1, T_f, d_s, d_f, d_w, d_δ and a symmetric matrix $\mathbf{R} > 0$, the closed-loop controlled system (35) is FTB with respect to (c_1, c_2, T_f, $\mathbf{R}$, d_s, d_f, d_w, d_δ) and satisfies (42) for all admissible $\mathbf{w}(t)$, if there exist positive constants c_2, $\gamma_f > \gamma_n$, η, τ, symmetric positive-definite matrix $\tilde{\mathbf{P}}^{-j}$ for any $\boldsymbol{\rho}$ and any appropriately dimensioned matrices $\mathbf{L}$, which satisfy

$$\begin{bmatrix} \boldsymbol{\Omega}_3 & \mathbf{Z}^{\mathrm{T}} & \mathbf{0} & \chi^{-1}\mathbf{Z}^{\mathrm{T}}\mathbf{c}_1^{\mathrm{T}} & \mathbf{0} & \mathbf{0} & \mathbf{0} \\ * & \boldsymbol{\Omega}_4 & \mathbf{B}_1 & \mathbf{0} & (\mathbf{I}+\mathbf{M})\mathbf{B}\boldsymbol{\rho}\mathbf{L} & \mathbf{0} & \tilde{P}^{-j} \\ * & * & -\gamma_0^2 & \mathbf{0} & \mathbf{0} & \mathbf{0} & \mathbf{0} \\ * & * & * & \hat{\boldsymbol{\Omega}} & \mathbf{0} & \mathbf{0} & \mathbf{0} \\ * & * & * & * & -\mathbf{Z}-\mathbf{Z}^{\mathrm{T}} & \mathbf{G}\tilde{\mathbf{P}}^{-j}-\mathbf{Z} & \mathbf{0} \\ * & * & * & * & * & -\mathbf{J}^j & \mathbf{0} \\ * & * & * & * & * & * & \bar{\boldsymbol{\Omega}} \end{bmatrix} < 0, \tag{52}$$

$$\frac{c_1}{\lambda_{\min}(\mathbf{P}^j)} + (d_s + d_f + d_w + d_\delta) < \frac{c_2 e^{-\alpha_0 t}}{\lambda_{\max}(\mathbf{P}^j)}, \tag{53}$$

where $\boldsymbol{\Omega}_3 = \chi^{-1}(\tilde{\mathbf{P}}^{-j} - \mathbf{Z} - \mathbf{Z}^{\mathrm{T}})$, $\boldsymbol{\Omega}_4 = \mathbf{A}\tilde{\mathbf{P}}^{-j} + \tilde{\mathbf{P}}^{-j}\mathbf{A}^{\mathrm{T}} - (\chi + \alpha_0)\tilde{\mathbf{P}}^{-j} + \tau^{-1} + \mathbf{J}^j + (\mathbf{I}+\mathbf{M})\mathbf{B}\boldsymbol{\rho}\mathbf{L} + [(\mathbf{I}+\mathbf{M})\mathbf{B}\boldsymbol{\rho}\mathbf{L}]^{\mathrm{T}}$, $\hat{\boldsymbol{\Omega}} = -\mathbf{I} - \chi^{-1}\mathbf{c}_1\tilde{\mathbf{P}}^{-j}\mathbf{c}_1^{\mathrm{T}}$, $\bar{\boldsymbol{\Omega}} = -(\frac{1}{\eta} + \tau L_g^2)^{-1}$; $\gamma_0 = \gamma_n$ and $\gamma_0 = \gamma_f$ denote the adaptive H_∞ performance bounds for the normal case and fault cases of the closed-loop FTC system (35), respectively; then the adaptive closed-loop system (35) will exists an FTC H_∞ controller.

Proof: Select the same Lyapunov function candidate as Theorem 1 and define the following function:

$$\begin{aligned} J_2 &= V(\mathbf{x}(t)) + \sum_{i=1}^{2}\rho_i\tilde{\mathbf{K}}_{1i}^{\mathrm{T}}(t)\Gamma_i^{-1}\tilde{\mathbf{K}}_{1i}(t) + r_1^{-1}\tilde{k}_4^2(t) \\ &\quad + \frac{1}{2}\mu r_2^{-1}\tilde{k}_5^2(t) + r_3^{-1}\tilde{\mathbf{W}}^{\mathrm{T}}\tilde{\mathbf{W}}, \end{aligned} \tag{54}$$

$$J_3 = \dot{J}_2 - \alpha_0\mathbf{x}^{\mathrm{T}}(t)\tilde{\mathbf{P}}^j\mathbf{x}(t) + \mathbf{y}^{\mathrm{T}}(t)\mathbf{y}(t) - \gamma_0^2\mathbf{w}^{\mathrm{T}}(t)\mathbf{w}(t). \tag{55}$$

Then, according to (22), (35), (31)-(34), J_3 can be written as

$$\begin{aligned} J_3 =& \mathbf{x}^{\mathrm{T}}(t)\tilde{\mathbf{P}}^j[\mathbf{A} + \Delta\mathbf{A} + \mathbf{B}\boldsymbol{\rho}(\hat{\mathbf{K}}_1(t) + \mathbf{K}_2(t) + \mathbf{K}_3(t))\mathbf{G} \\ &+ \Delta\mathbf{B}\boldsymbol{\rho}(\hat{\mathbf{K}}_1(t) + \mathbf{K}_2(t) + \mathbf{K}_3(t))\mathbf{G}]\mathbf{x}(t) + [\mathbf{A} + \Delta\mathbf{A} \\ &+ \mathbf{B}\boldsymbol{\rho}(\hat{\mathbf{K}}_1(t) + \mathbf{K}_2(t) + \mathbf{K}_3(t))\mathbf{G} + \Delta\mathbf{B}\boldsymbol{\rho}(\hat{\mathbf{K}}_1(t) \\ &+ \mathbf{K}_2(t) + \mathbf{K}_3(t))\mathbf{G}]^{\mathrm{T}}\tilde{\mathbf{P}}^j\mathbf{x}(t) \\ &+ 2\mathbf{x}^{\mathrm{T}}(t)\tilde{\mathbf{P}}^j(\mathbf{B} + \Delta\mathbf{B})\boldsymbol{\rho}\bar{\boldsymbol{\delta}}_{\mathbf{u}}(\mathbf{x}) \\ &+ 2\mathbf{x}^{\mathrm{T}}(t)\tilde{\mathbf{P}}^j(\mathbf{B} + \Delta\mathbf{B})\mathbf{u}_s(t) + 2\mathbf{x}^{\mathrm{T}}(t)\tilde{\mathbf{P}}^j f(t,\mathbf{x}) \\ &+ 2\mathbf{x}^{\mathrm{T}}(t)\tilde{\mathbf{P}}^j\mathbf{B}\mathbf{F}\mathbf{w}(t) - \alpha_0 x^{\mathrm{T}}(t)\tilde{\mathbf{P}}^j\mathbf{x}(t) \\ &+ x^{\mathrm{T}}(t)\mathbf{c}_1^{\mathrm{T}}\mathbf{c}_1\mathbf{x}(t) - \gamma_0^2\mathbf{w}^{\mathrm{T}}(t)\mathbf{w}(t) \\ &- 2\sum_{i=1}^{2}\rho_i\tilde{\mathbf{K}}_{1i}^{\mathrm{T}}(t)\Gamma_i^{-1}\dot{\hat{\mathbf{K}}}_{1i}(t) - 2r_1^{-1}\tilde{k}_4(t)\dot{\hat{k}}_4(t) \\ &- \mu r_2^{-1}\tilde{k}_5(t)\dot{\hat{k}}_5(t) - 2r_3^{-1}\tilde{\mathbf{W}}^{\mathrm{T}}\dot{\hat{\mathbf{W}}}. \end{aligned} \tag{56}$$

For arbitrary positive constant $\tau \geq 0$, γ_0, ε_τ, ε_f and L_g, employing the well-known Young's inequality $2x^{\mathrm{T}}y \leq \varepsilon_i x^{\mathrm{T}}x + \varepsilon_i^{-1}y^{\mathrm{T}}y$ and Lipschitz condition, we have

$$\begin{cases} \left\|\mathbf{x}^{\mathrm{T}}(t)\tilde{\mathbf{P}}^j\mathbf{B}\right\|\|\mathbf{x}(t)\| \leq l^*(\eta l^*\left\|\mathbf{x}^{\mathrm{T}}(t)\tilde{\bar{\mathbf{P}}}^j\mathbf{B}\right\|^2 \\ \qquad\qquad + \dfrac{1}{\eta l^*}\|\mathbf{x}(t)\|^2) \\ 2\left\|\mathbf{x}^{\mathrm{T}}(t)\tilde{\mathbf{P}}^j f(t,\mathbf{x})\right\| \leq \tau^{-1}\left\|\mathbf{x}^{\mathrm{T}}(t)\tilde{\mathbf{P}}^j\right\|^2 \\ \qquad\qquad + \tau L_g^2\left\|\mathbf{x}^{\mathrm{T}}(t)\right\|^2 \\ 2\mathbf{x}^{\mathrm{T}}(t)\tilde{\mathbf{P}}^j\mathbf{B}_1\mathbf{w}(t) \leq \gamma_0^{-2}\mathbf{x}^{\mathrm{T}}(t)\tilde{\mathbf{P}}^j\mathbf{B}_1\mathbf{B}_1^{\mathrm{T}}\tilde{\mathbf{P}}^j\mathbf{x}(t) \\ \qquad\qquad + \gamma_0^2\mathbf{w}^{\mathrm{T}}(t)\mathbf{w}(t). \end{cases} \tag{57}$$

Using (19), (22), (26), (27), (34), (35), (40), (41), and (57), equation (56) can be written as

$$\begin{aligned} J_3 \leq& \mathbf{x}^{\mathrm{T}}(t)[\tilde{\mathbf{P}}^j[\mathbf{A} + (\mathbf{I}+\mathbf{M})\mathbf{B}\boldsymbol{\rho}\mathbf{K}_1\mathbf{G}] \\ &+ [\mathbf{A} + (\mathbf{I}+\mathbf{M})\mathbf{B}\boldsymbol{\rho}\mathbf{K}_1\mathbf{G}]^{\mathrm{T}}\tilde{\mathbf{P}}^j - \alpha_0\tilde{\mathbf{P}}^j + \tau^{-1}\tilde{\mathbf{P}}^j\tilde{\mathbf{P}}^j \\ &+ \tau L_g^2 + \frac{1}{\eta}\mathbf{I} + \gamma_0^{-2}\tilde{\mathbf{P}}^j\mathbf{B}_1\mathbf{B}_1^{\mathrm{T}}\tilde{\mathbf{P}}^j + \mathbf{c}_1^{\mathrm{T}}\mathbf{c}_1]\mathbf{x}(t) \\ &- 2\mathbf{x}^{\mathrm{T}}(t)\tilde{\mathbf{P}}^j(\mathbf{I}+\mathbf{M})\mathbf{B}\boldsymbol{\rho}\tilde{\mathbf{K}}_1(t)\mathbf{G}\mathbf{x}(t) \\ &- 2(1+\theta_1)\left\|\mathbf{x}^{\mathrm{T}}(t)\tilde{\bar{\mathbf{P}}}^j\mathbf{B}\right\|\tilde{k}_4(t) \\ &- (1+\theta_1)\mu\eta\left\|\mathbf{x}^{\mathrm{T}}(t)\tilde{\bar{\mathbf{P}}}^j\mathbf{B}\right\|^2\tilde{k}_5(t)I \\ &+ 2\mathbf{x}^{\mathrm{T}}(t)\tilde{\mathbf{P}}^j(+\mathbf{M})\mathbf{B}\boldsymbol{\rho}\tilde{\mathbf{W}}^{\mathrm{T}}\mathbf{h}(\mathbf{x}) \\ &- 2\sum_{i=1}^{2}\rho_i\tilde{\mathbf{K}}_{1i}^{\mathrm{T}}(t)\Gamma_i^{-1}\dot{\hat{\mathbf{K}}}_{1i}(t) - 2r_1^{-1}\tilde{k}_4(t)\dot{\hat{k}}_4(t) \\ &- \mu r_2^{-1}\tilde{k}_5(t)\dot{\hat{k}}_5(t) - 2r_3^{-1}\tilde{\mathbf{W}}^{\mathrm{T}}\dot{\hat{\mathbf{W}}}. \end{aligned} \tag{58}$$

Set

$$\begin{aligned} &\tilde{\mathbf{P}}^j[\mathbf{A} + (\mathbf{I}+\mathbf{M})\mathbf{B}\boldsymbol{\rho}\mathbf{K}_1\mathbf{G}] + [\mathbf{A} + (\mathbf{I}+\mathbf{M})\mathbf{B}\boldsymbol{\rho}\mathbf{K}_1\mathbf{G}]^{\mathrm{T}}\tilde{\mathbf{P}}^j \\ &\quad - \alpha_0\tilde{\mathbf{P}}^j + \tau^{-1}\tilde{\mathbf{P}}^j\tilde{\mathbf{P}}^j + \tau L_g^2 + \frac{1}{\eta}\mathbf{I} \\ &\quad + \gamma_0^{-2}\tilde{\mathbf{P}}^j\mathbf{B}_1\mathbf{B}_1^{\mathrm{T}}\tilde{\mathbf{P}}^j + \mathbf{c}_1^{\mathrm{T}}\mathbf{c}_1 < 0. \end{aligned} \tag{59}$$

Then, applying (43), equation (59) can be further changed to be

$$\begin{bmatrix} \boldsymbol{\Omega}_1 & \tilde{\mathbf{P}}^j\mathbf{B}_1 & \mathbf{c}_1^{\mathrm{T}} & \mathbf{I} \\ * & -\gamma^2 & \mathbf{0} & \mathbf{0} \\ * & * & -\mathbf{I} & \mathbf{0} \\ * & * & * & \bar{\boldsymbol{\Omega}} \end{bmatrix} < \mathbf{0}, \tag{60}$$

where $\boldsymbol{\Omega}_1 = \tilde{\mathbf{P}}^j\mathbf{A} + \mathbf{A}^{\mathrm{T}}\tilde{\mathbf{P}}^j - \alpha_0\tilde{\mathbf{P}}^j + \tau^{-1}\tilde{\mathbf{P}}^j\tilde{\mathbf{P}}^j + \tilde{\mathbf{P}}^j(\mathbf{I}+\mathbf{M})\mathbf{B}\boldsymbol{\rho}\mathbf{K}_1\mathbf{G} + [(\mathbf{I}+\mathbf{M})\mathbf{B}\boldsymbol{\rho}\mathbf{K}_1\mathbf{G}]^{\mathrm{T}}\tilde{\mathbf{P}}^j$, $\bar{\boldsymbol{\Omega}} = -(\frac{1}{\eta} + \tau L_g^2)^{-1}$.

Pre- and post-multiplying the inequality (60) by block-diagonal matrix $diag(\tilde{\mathbf{P}}^{-j}, \mathbf{I}, \ldots, \mathbf{I})$ and for any positive constant $\chi > 0$, equation (60) can be further changed to be

$$\begin{bmatrix} \boldsymbol{\Omega}_2 - \chi\tilde{\mathbf{P}}^{-j} & \mathbf{B}_1 & \mathbf{0} & \tilde{\mathbf{P}}^{-j} \\ * & -\gamma_0^2 & \mathbf{0} & \mathbf{0} \\ * & * & \hat{\Omega} & \mathbf{0} \\ * & * & * & \bar{\Omega} \end{bmatrix} + \boldsymbol{\Lambda}^{\mathrm{T}}\chi\tilde{\mathbf{P}}^{-j}\boldsymbol{\Lambda} < \mathbf{0}, \tag{61}$$

where $\boldsymbol{\Omega}_2 = \mathbf{A}\tilde{\mathbf{P}}^{-j} + \tilde{\mathbf{P}}^{-j}\mathbf{A}^{\mathrm{T}} - \alpha_0\tilde{\mathbf{P}}^{-j} + \tau^{-1} + (\mathbf{I}+\mathbf{M})\mathbf{B}\rho\mathbf{K}_1\mathbf{G}\tilde{\mathbf{P}}^{-j} + [(\mathbf{I}+\mathbf{M})\mathbf{B}\rho\mathbf{K}_1\mathbf{G}\tilde{\mathbf{P}}^{-j}]^{\mathrm{T}}$, $\boldsymbol{\Lambda} = [\mathbf{I} \quad \mathbf{0} \quad \chi^{-1}\mathbf{c}_1^{\mathrm{T}} \quad \mathbf{0}]$, $\hat{\Omega} = -\mathbf{I} - \chi^{-1}\mathbf{c}_1\tilde{\mathbf{P}}^{-j}\mathbf{c}_1^{\mathrm{T}}$. Then, applying (43) and pre- and post-multiplying both sides by $diag(\mathbf{Z}^{\mathrm{T}}, \mathbf{I}, \ldots, \mathbf{I})$, equation (61) can be written as

$$\begin{bmatrix} -\chi^{-1}\mathbf{Z}^{\mathrm{T}}\tilde{\mathbf{P}}^{j}\mathbf{Z} & \mathbf{Z}^{\mathrm{T}} & \mathbf{0} & \chi^{-1}\mathbf{Z}^{\mathrm{T}}\mathbf{c}_1^{\mathrm{T}} & \mathbf{0} \\ * & \boldsymbol{\Omega}_2 - \chi\tilde{\mathbf{P}}^{-j} & \mathbf{B}_1 & \mathbf{0} & \tilde{\mathbf{P}}^{-j} \\ * & * & -\gamma_0^2 & \mathbf{0} & \mathbf{0} \\ * & * & * & \hat{\Omega} & \mathbf{0} \\ * & * & * & * & \bar{\Omega} \end{bmatrix} < \mathbf{0}. \tag{62}$$

Due to $\mathbf{Z}^{\mathrm{T}}\tilde{\mathbf{P}}^{j}\mathbf{Z} \geq \mathbf{Z} + \mathbf{Z}^{\mathrm{T}} - \tilde{\mathbf{P}}^{-j}$, equation (62) can be written as

$$\begin{bmatrix} \boldsymbol{\Omega}_3 & \mathbf{Z}^{\mathrm{T}} & \mathbf{0} & \chi^{-1}\mathbf{Z}^{\mathrm{T}}\mathbf{c}_1^{\mathrm{T}} & \mathbf{0} \\ * & \boldsymbol{\Omega}_2 - \chi\tilde{\mathbf{P}}^{-j} & \mathbf{B}_1 & \mathbf{0} & \tilde{\mathbf{P}}^{-j} \\ * & * & -\gamma_0^2 & \mathbf{0} & \mathbf{0} \\ * & * & * & \hat{\Omega} & \mathbf{0} \\ * & * & * & * & \bar{\Omega} \end{bmatrix} < \mathbf{0}, \tag{63}$$

where $\boldsymbol{\Omega}_3 = \chi^{-1}(\tilde{\mathbf{P}}^{-j} - \mathbf{Z} - \mathbf{Z}^{\mathrm{T}})$. From (63) we have

$$\begin{aligned} \boldsymbol{\Omega}_2 - \chi\tilde{\mathbf{P}}^{-j} =& [\mathbf{A} + (\mathbf{I}+\mathbf{M})\mathbf{B}\rho\mathbf{K}_1\mathbf{G}]\tilde{\mathbf{P}}^{-j} \\ &+ \tilde{\mathbf{P}}^{-j}[\mathbf{A} + (\mathbf{I}+\mathbf{M})\mathbf{B}\rho\mathbf{K}_1\mathbf{G}]^{\mathrm{T}} \\ &- \chi\tilde{\mathbf{P}}^{-j} - \alpha_0\tilde{\mathbf{P}}^{-j} + \tau^{-1} \\ =& A\tilde{\mathbf{P}}^{-j} + \tilde{\mathbf{P}}^{-j}\mathbf{A}^{\mathrm{T}} - (\chi + \alpha_0)\tilde{\mathbf{P}}^{-j} + \tau^{-1} \\ &+ \mathbf{J}^j + (\mathbf{I}+\mathbf{M})\mathbf{B}\rho\mathbf{L} + [(\mathbf{I}+\mathbf{M})\mathbf{B}\rho\mathbf{L}]^{\mathrm{T}} \\ &+ (\mathbf{I}+\mathbf{M})\mathbf{B}\rho\mathbf{L}\mathbf{Z}^{-1}(\mathbf{G}\tilde{\mathbf{P}}^{-j} - \mathbf{Z}) \\ &+ [(\mathbf{I}+\mathbf{M})\mathbf{B}\rho\mathbf{L}\mathbf{Z}^{-1}(\mathbf{G}\tilde{\mathbf{P}}^{-j} - \mathbf{Z})]^{\mathrm{T}} - \mathbf{J}^j. \end{aligned} \tag{64}$$

Due to

$$\begin{aligned} &(\mathbf{I}+\mathbf{M})\mathbf{B}\rho\mathbf{L}\mathbf{Z}^{-1}(\mathbf{G}\tilde{\mathbf{P}}^{-j} - \mathbf{Z}) \\ &\quad + [(\mathbf{I}+\mathbf{M})\mathbf{B}\rho\mathbf{L}\mathbf{Z}^{-1}(\mathbf{G}\tilde{\mathbf{P}}^{-j} - \mathbf{Z})]^{\mathrm{T}} - \mathbf{J}^j \\ &\leq (\mathbf{I}+\mathbf{M})\mathbf{B}\rho\mathbf{L}\mathbf{Z}^{-1}(\mathbf{G}\tilde{\mathbf{P}}^{-j} - \mathbf{Z})\mathbf{J}^{-j} \\ &\quad \times [(\mathbf{I}+\mathbf{M})\mathbf{B}\rho\mathbf{L}\mathbf{Z}^{-1}(\mathbf{G}\tilde{\mathbf{P}}^{-j} - \mathbf{Z})]^{\mathrm{T}}. \end{aligned} \tag{65}$$

Then, applying (43), equation (64) can be written as

$$\begin{bmatrix} \boldsymbol{\Omega}_4 & (\mathbf{I}+\mathbf{M})\mathbf{B}\rho\mathbf{L} & \mathbf{0} \\ * & -\mathbf{Z} - \mathbf{Z}^{\mathrm{T}} & \mathbf{G}\tilde{\mathbf{P}}^{-j} - \mathbf{Z} \\ * & * & -\mathbf{J}^j \end{bmatrix} < \mathbf{0}, \tag{66}$$

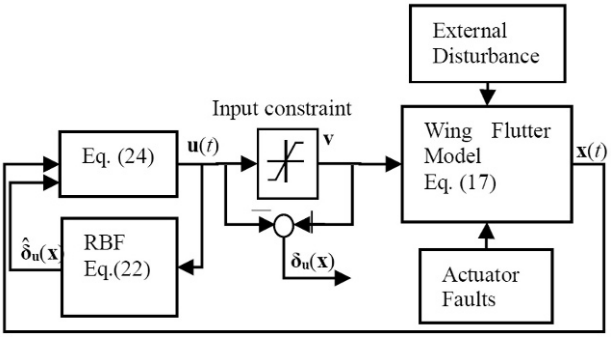

Fig. 5. The closed-loop flutter system with the compensation control scheme.

where $\boldsymbol{\Omega}_4 = \mathbf{A}\tilde{\mathbf{P}}^{-j} + \tilde{\mathbf{P}}^{-j}\mathbf{A}^{\mathrm{T}} - (\chi + \alpha_0)\tilde{\mathbf{P}}^{-j} + \tau^{-1} + \mathbf{J}^j + (\mathbf{I}+\mathbf{M})\mathbf{B}\rho\mathbf{L} + [(\mathbf{I}+\mathbf{M})\mathbf{B}\rho\mathbf{L}]^{\mathrm{T}}$.

From (66), equation (63) can be written as

$$\begin{bmatrix} \boldsymbol{\Omega}_3 & \mathbf{Z}^{\mathrm{T}} & \mathbf{0} & \chi^{-1}\mathbf{Z}^{\mathrm{T}}\mathbf{c}_1^{\mathrm{T}} & \mathbf{0} & \mathbf{0} & \mathbf{0} \\ * & \boldsymbol{\Omega}_4 & \mathbf{B}_1 & 0 & (\mathbf{I}+\mathbf{M})\mathbf{B}\rho\mathbf{L} & \mathbf{0} & \tilde{\mathbf{P}}^{-j} \\ * & * & -\gamma_0^2 & \mathbf{0} & \mathbf{0} & \mathbf{0} & \mathbf{0} \\ * & * & * & \hat{\Omega} & \mathbf{0} & \mathbf{0} & \mathbf{0} \\ * & * & * & * & -\mathbf{Z} - \mathbf{Z}^{\mathrm{T}} & \mathbf{G}\tilde{\mathbf{P}}^{-j} - \mathbf{Z} & \mathbf{0} \\ * & * & * & * & * & -\mathbf{J}^j & \mathbf{0} \\ * & * & * & * & * & * & \bar{\Omega} \end{bmatrix} < \mathbf{0}. \tag{67}$$

From (25), (28), (29), (30) and (67), equation (58) can be written as $J_3 \leq 0$, which implies that the flutter system is ultimately uniformly bounded, and the flutter state $x(t)$ converges to zero.

Algorithm: Assume that LMIs (52) and Eq. (53) are satisfied, control gain $\mathbf{K}_2(t)$, $\mathbf{K}_3(t)$, adaptive update laws $\hat{\mathbf{K}}_{1i}(t)$, $\hat{k}_4(t)$ $\hat{k}_5(t)$ and $\hat{\mathbf{W}}$ are given by (26), (27), (25), (28), (29) and (30), then the closed-loop flutter system (35) is stable, then γ_n and γ_f are minimized if the following optimization problem is solvable

$$\min \ \alpha_n\gamma_n^2 + \alpha_f\gamma_f^2, \text{ s.t. (52) and (53)}, \tag{68}$$

where α_n and α_f are weighting coefficients. Since the systems are operating under the normal condition most of time, we can choose $\alpha_n > \alpha_f$ in (68). A graphical representation of the flutter control with the proposed AFTC scheme is presented in Fig. 5

5. NUMERICAL SIMULATIONS

In this section, a numerical example is provided to illustrate the validity of our proposed approaches. The flutter of two-dimensional nonlinear wing is used as numerical example given in (17). The wing structural parameters are chosen as $s_\beta = 1.6$ m, $V = 1406$ m/s, $c = 0.7$ m, $\rho_1 = 0.0644$ Kg/m^3, $m_W = 1320$ Kg, $m_e = 490$ Kg, $e_{n1} = 10$,

$K_h = 2\times10^6$ N/m, $K_\theta = 2000$ Nm/rad, $x_C = 0.525$ m, $x_P = 0.28$ m, $I_C = 13205$ Kg.m^2, $\kappa = 1.4$ and $M_{\dot\theta} = -1.2$.

To demonstrate the superior performance of the proposed control scheme, the reentry vehicle is assumed to experience the following faulty case: before 4th second, the system operates in normal case, that is, all of the two actuators are normal. Between the 4th and the 10th second, the first actuator is float at $u_s(t) = 30+30\sin(0.1t)+20\cos(0.5t)$ and other actuator is loss of effectiveness, that is, $\rho_2 = 1-0.05t$ until loss effectiveness of 50%. After the 10th second, the second actuator has float and other actuator is loss of effectiveness, that is, $\rho_1 = 1-0.01t$ until loss effectiveness of 70%. The perturbations $\mathbf{w}(t) = [-10\sin(0.1\times t),\ 15]^{\mathrm{T}}$ enter into the systems at the beginning ($t \geq 0$).

To implement the controller, control and adaptation gains were selected by trial-and-error until a good performance was obtained. The controller parameters θ_1, b_N, η, Γ_i, r_1, $r_2$and r_3 in (20), (22), (27), (25), (28), (29) and (30) are chosen as

$$\theta_1 = 0.45,\ \ \eta = 100,\ \ r_1 = 0.25,\ \ r_2 = 0.25,$$
$$r_3 = 4.5,\ \ b_N = 5,\ \ \Gamma_i = 0.45.$$

The parameters $N(t)$, M, F, c_N and the initial values of the state $x(t)$ in (19), (22) and (17) are $\mathbf{N}(t) = \begin{bmatrix} 0.5\times\sin(t) & 0 & 0 & 0 \\ 0 & 0 & 0 & 0 \end{bmatrix}$, $\mathbf{F} = \begin{bmatrix} 1.5 & -2 \\ 1 & -1 \end{bmatrix}^{\mathrm{T}}$, $\mathbf{M} = \begin{bmatrix} 0.5 & 0 & 0 & 0 \\ 0 & 0.5 & 0 & 0 \\ 0 & 0 & 0.5 & 0 \\ 0 & 0 & 0 & 0.5 \end{bmatrix}$, $\mathbf{c}_N = \begin{bmatrix} -1 & -0.5 & 0 & 0.5 & 1 \\ -1 & -0.5 & 0 & 0.5 & 1 \end{bmatrix}$, $\mathbf{x}(0) = [0,\ 0.5,\ 0,\ 0.5]^{\mathrm{T}}$.

Considering the above-mentioned faulty cases and using the finite-time H_∞ adaptive state feedback controller designed in this paper for flutter of the wing. By using Algorithm with $\alpha_n = 5$, $\alpha_f = 1$, we obtain H_∞ performances of the closed-loop system as 0.3923 (normal) and 1.3553 (fault). Considering the above-mentioned faulty cases and using the finite-time H_∞ adaptive state feedback controller designed in this paper for flutter of the wing, Fig. 6 shows that the state variable $\mathbf{x}(t)$ and control input $\mathbf{u}(t)$ of wing flutter. As shown in Fig. 6, the proposed controller can make the system stable when the actuator and sensor faults occur. Figs. 7-8 show the results of robustness about the mass variation of the reentry vehicle wing and the variation of torsion stiffness coefficient. Fig. 7(a) shows the simulation results of the reentry vehicle wing according to its real mass by the controller. Plunge displacement and torsion angle will be given in Fig. 7(a), which are two changing states of system. We know that the controller designed by real mass will ensure the stabilization of the system state. Fig. 7(b) shows the simulation results of -15% mass variation of the reentry vehicle wing. In other

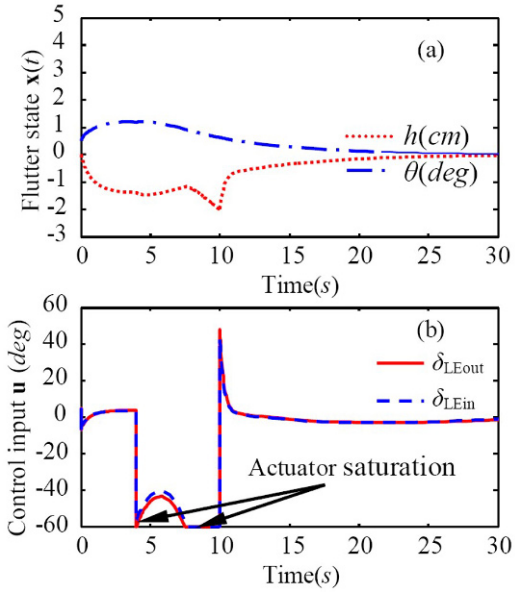

Fig. 6. Time response of the airfoil states $\mathbf{x}$ and control input $\mathbf{u}$ in case of fault.

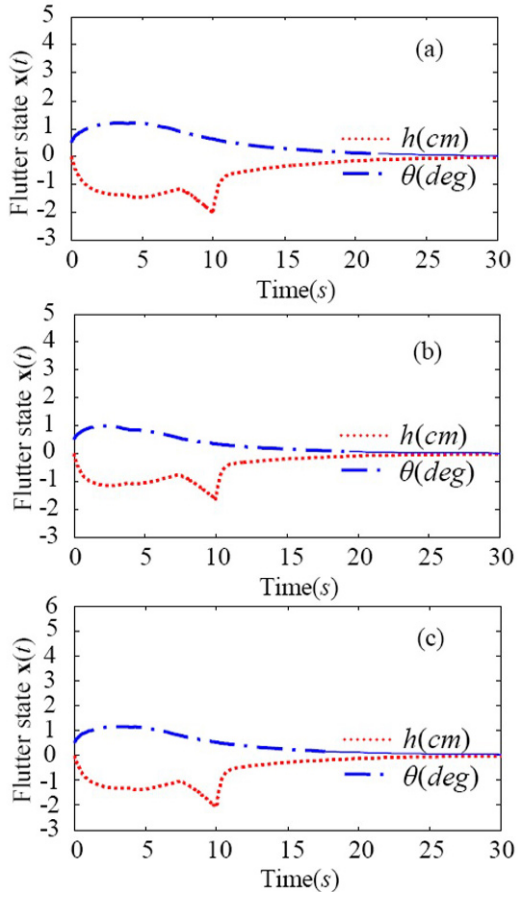

Fig. 7. Robustness of controller with respect to mass variance of reentry vehicle: (a) $m = 1320$ Kg, (b) $-15\%\times m$, (c) $+15\%\times m$.

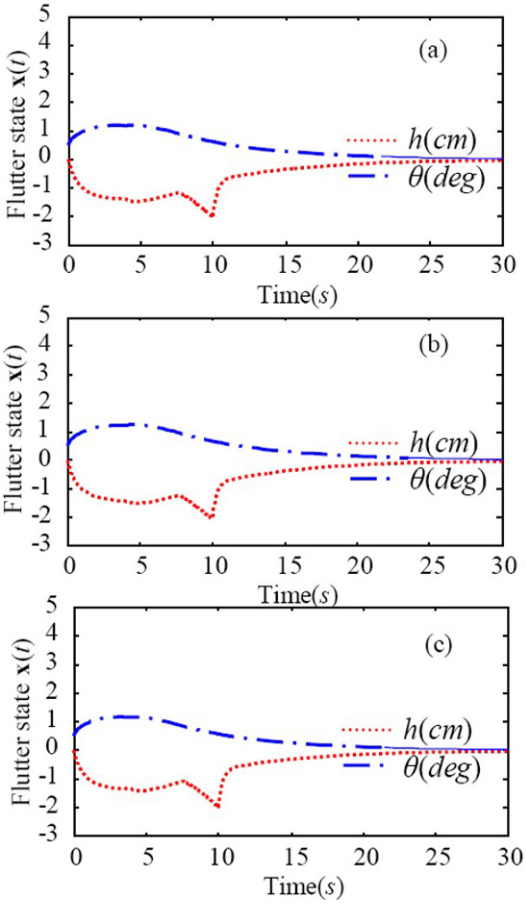

Fig. 8. Robustness of controller with respect to torsion stiffness coefficient variance of reentry vehicle: (a) $K_\theta = 2\times10^4$, (b) $-15\%\times K_\theta$, (c) $+15\%\times K_\theta$.

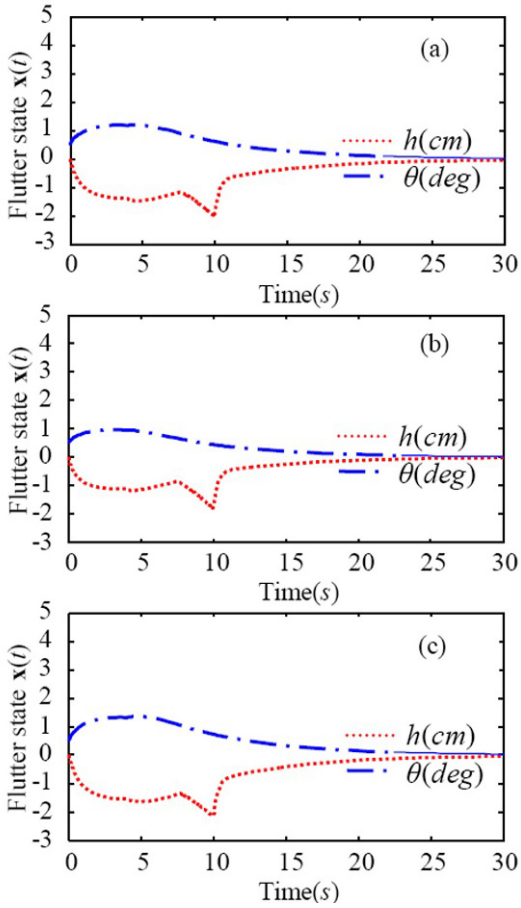

Fig. 9. Robustness of controller with respect to disturbance variance of reentry vehicle: (a) $\mathbf{w}(t) = [-10\sin(0.1\times t),\ 15]^{\mathrm{T}}$, (b) $-50\%\times\mathbf{w}(t)$, (c) $+50\%\times\mathbf{w}(t)$.

words, the controller will be designed by $-15\%\times m$ (m is the real mass of the reentry vehicle wing) for the system which the real mass is m. From the results of Fig. 7(b), the controller designed in this paper will effectively suppress the response of the system when the mass variation of the reentry vehicle wing is -15%. Fig. 7(c) shows that the control law will also be effective when the mass variation is +15%. From Fig. 7 we know that the controller designed in this paper shows great robustness about the system mass. Fig. 8 shows the robustness about variation of the torsion stiffness coefficient K_θ of the controller, which considers the $\pm15\%$ variation of the K_θ. To sum up, the controller designed in this paper shows great robustness of variation of the structural parameters.

Fig. 9 shows the results of robustness of the controller about the variation of system disturbance. Fig. 9(a) shows the simulation results when the controller is set with the disturbance value (that is $\mathbf{w}(t)$ in (18), which is $\mathbf{w}(t) = [-10\sin(0.1\times t),\ 15]^T$) we designed. Two system states (plunge displacement and torsion angle) can be kept stable under this controller. Fig. 9(b) is the simulation result of -50% external disturbance variation. In other word, the controller is designed under $-50\%\times\mathbf{w}(t)$ ($\mathbf{w}(t)$ is the true value of the disturbance we set, $\mathbf{w}(t) = [-10\sin(0.1\times t),\ 15]^T$), then we apply this controller in the system whose external disturbance is $\mathbf{w}(t)$. From Fig. 9(b) we can see that the controller we designed can suppress the response of the system effectively when the variation of external disturbance is -50%. Fig. 9(c) is the simulation result of $+50\%$ external disturbance variation, which can show that our controller is still effective. From the simulation results in Fig. 9, we can see clearly that the controller we designed has good robustness to external disturbance of the system.

The finite-time closed-loop FTC system with external disturbances and parameter uncertainties can be ensured to be asymptotically stable in the presence of actuator and sensor faults. The sensor and actuator faults are both considered including loss of effectiveness, stuck and outage of actuator, and loss of effectiveness of sensor. All the simulation results verify that the proposed control approach is

effective.

6. CONCLUSIONS

Based on the trajectory optimization, a novel finite-time H_∞ adaptive fault-tolerant control design scheme is proposed for wing flutter of reentry vehicle subject to input saturation, external disturbances and parameter uncertainties. The input saturation is approximated by a radial basis function. Sensor and actuator faults are both considered, including loss of effectiveness, stuck and outage of actuator, and loss of effectiveness of sensor. The proposed finite-time H_∞ adaptive fault-tolerant controller is proved to adaptively adjust controller parameters to compensate the faults, disturbances and parameter uncertainties within the system, and all the signals in the closed-loop system are bounded in probability. Numerical simulation results further illustrate the effectiveness of the presented approach.

REFERENCES

[1] A. E. Thomas, "Fluid/chemistry modeling for hypersonic flight analysis," *Computers Math Applications*, vol. 24, no. 5/6, pp. 25-36, September 1992. [click]

[2] A. Mazzaracchio and M. Marchetti, "Aprobabilistic sizing tool and monte carlo analysis for entry vehicle ablative thermal protection systems," *Acta Astronautica*, vol. 66, no. 5/6, pp. 821-835, March 2010. [click]

[3] Y. H. Zhao, "Flutter suppression of a high aspect-ratio wing with multiple control surfaces," *Journal of Sound and Vibration*, vol. 324, no. 3, pp. 490-513, July 2009.

[4] Z. Wang, A. Behal, and P. Marzocca, "Model-free control design for multi-input multi-output aerolastic system subject to external disturbance," *Journal of Guidance, Control, and Dynamics*, vol. 34, no. 2, pp. 446-458, March-April 2011. [click]

[5] Z. Wang, A. Behal, and P. Marzocca, "Continuous robust control for two-dimensional airfoils with leading and trailing-edge flaps," *Journal of Guidance, Control, and Dynamics*, vol. 35, no. 2, pp. 510-519, March-April 2012. [click]

[6] K. Zhang, Z. Wang, A. Behal, and P. Marzocca, "Novel nonlinear control design for a two-dimensional airfoil under unsteady flow," *Journal of Guidance, Control, and Dynamics*, vol. 36, no. 6, pp. 1681-1694, November-December 2013. [click]

[7] M. Cassaro and M. Battipede, "Comparison of adaptive control architectures for flutter suppression," *Journal of Guidance, Control, and Dynamics*, vol. 38, no. 2, pp. 346-354, February 2015.

[8] X. J. Li and G. H. Yang, "Robust adaptive fault-tolerant control for uncertain linear systems with actuator failures," *IET Control Theory and Applications*, vol. 6, no. 10, pp. 1544-1551, February 2012.

[9] M. Blanke, R. Izadi-Zamanabadi, and S. A. Bosh, "Fault-tolerant control systems-A holistic view," *Control Engineering Practice*, vol. 5, no. 5, pp. 693-702, May 1997. [click]

[10] A. Zolghadri, "Advanced model-based FDIR techniques for aerospace systems: Today challenges and opportunities," *Progress in Aerospace Sciences*, vol. 53, pp. 18-29, August 2012. [click]

[11] Q. Shen, D. W. Wang, and S. Q. Zhu, "Integral-type sliding mode fault-tolerant control for attitude stabilization of spacecraft," *IEEE Transactions on Control Systems Technology*, vol. 23, no. 3, pp. 1041-1051, May 2015.

[12] Q. Shen, D. W. Wang, S. Q. Zhu, and E. K. Poh, "Inertia-free fault-tolerant spacecraft attitude tracking using control allocation," *Automatica*, vol. 62, pp. 114-121, December 2015. [click]

[13] B. Xu, Y. Y. Guo, Y. Yuan, Y. H. Fan, and D. W. Wang, "Fault-tolerant control using command-filtered adaptive back-stepping technique: application to hypersonic longitudinal flight dynamics," *International Journal of Adaptive Control and Signal Processing*, vol. 30, pp. 553-577, August 2016.

[14] C. S. Liu, B. Jiang, and S. J. Zhang, "Fault-tolerant synthesis controller design for a flight-tracking system," *IET Control Theory and Applications*, vol. 5, no. 11, pp. 1243-1254, July 2011.

[15] L. I. Allerhand and U. Shaked, "Robust switching-based fault tolerant control," *IEEE Transactions on Automatic Control*, vol. 60, no. 8, pp. 2272-2276, August 2015.

[16] Q. X. Jia, W. Chen, Y. C. Zhang, and H. Y. Li, "Fault reconstruction and fault-tolerant control via learning observers in Takagi-Sugeno fuzzy descriptor systems with time delays," *IEEE Transactions on Industrial Electronics*, vol. 62, no. 6, pp. 114-121, June 2015.

[17] B. Xu, X. Y. Huang, D. W. Wang, and F. C. Sun, "Dynamic surface control of constrained hypersonic flight models with parameter estimation and actuator compensation," *Asian Journal of Control*, vol. 16, no. 1, pp. 162-174, January 2014.

[18] B. Xu, Z. K. Shi, and C. G. Yang, "Composite fuzzy control of a class of uncertain nonlinear systems with disturbance observer," *Nonlinear Dynamics*, vol. 80, no. 1-2, pp. 341-351, April 2015. [click]

[19] Y. Zhong, "Globally stable adaptive system design for minimum phase SISO plants with input saturation," *Automatica*, vol. 41, no. 9, pp. 1539-1547, September 2005. [click]

[20] N. D. S. Sarah and S. K. Nesrin, "Survey of planetary entry guidance algorithms," *Progress in Aerospace Sciences*, vol. 68, pp. 64-74, July 2014. [click]

[21] R. Jamilnia and A. Naghash, "Simultaneous optimization of staging and trajectory of launch vehicles using two different approaches," *Aerospace Science and Technology*, vol. 23, no. 1, pp. 85-92, December 2012. [click]

[22] B. L. Tian, Q. Zong, and J. Wang, "Quasi-continuous high-order sliding mode controller design for reusable launch vehicles in reentry phase," *Aerospace Science and Technology*, vol. 28, no. 1, pp. 198-207, July 2013. [click]

[23] D. Dirkx and E. Mooij, "Optimization of entry-vehicle shapes during conceptual design," *Acta Astronautica*, vol. 94, no. 1, pp. 198-214, January 2014. [click]

[24] L. Q. Zhou, Y. S. Chen, and F. Q. Chen, "Chaotic motions of a two-dimensional airfoil with cubic nonlinearity in supersonic flow," *Aerospace Science and Technology*, vol. 25, no. 1, pp. 138-144, March 2013. [click]

[25] Y. M. Chen, J. K. Liu, and G. Meng, "Equivalent damping of aeroelastic system of an wing with cubic stiffness," *Journal of Fluids and Structures*, vol. 27, no. 8, pp. 1447-1454, November 2011.

[26] J. N. Lu, H. P. Hu, and Y. P. Bai, "Generalized radial basis function neural network based on an improved dynamic particle swarm optimization and AdaBoost algorithm," *Neurocomputing*, vol. 152, no. 25, pp. 305-315, March 2015. [click]

[27] F. Amato and M. Ariola, "Finite-time control of linear systems subject to parametric uncertainties and disturbances," *Automatica*, vol. 37, no. 9, pp. 1459-1463, September 2001.

[28] Q. Y. Meng and Y. J. Shen, "Finite-time H_∞ control for linear continuous system with norm-bounded disturbance," *Communications in Nonlinear Science and Numerical Simulation*, vol. 14, no. 4, pp. 1043-1049, April 2009. [click]

[29] W. Zhang, H. S. Su, and H. W. Wang, "Full-order and reduced-order observers for one-sided Lipschitz nonlinear systems using Riccati equations," *Communications in Nonlinear Science and Numerical Simulation*, vol. 17, no. 12, pp. 4968-4977, December 2012. [click]

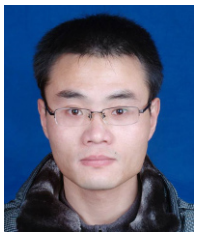

Ming-Zhou Gao is a Ph.D. candidate of Shanghai Jiaotong University, China. His major in Engineering Mechanics. His current research interests focus on structural dynamics and control.

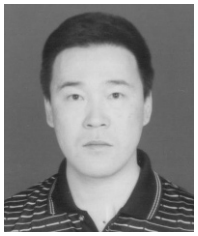

Guo-Ping Cai is a professor in the Department of Engineering Mechanics, Shanghai Jiaotong University, China. He received the Ph.D. degree in Engineering Mechanics from Xi'an Jiaotong University in 2000. His current research interests focus on structural dynamics and control, delayed system dynamics and control, and coupled system dynamics and control.